PHYSICS LETTERS B

Spectroscopy, lifetime and decay modes of the T_{bb}^- tetraquark

E. Hernández [a,*], J. Vijande [b], A. Valcarce [a], Jean-Marc Richard [c]

[a] *Departamento de Física Fundamental e IUFFyM, Universidad de Salamanca, 37008 Salamanca, Spain*
[b] *Unidad Mixta de Investigación en Radiofísica e Instrumentación Nuclear en Medicina (IRIMED), Instituto de Investigación Sanitaria La Fe (IIS-La Fe)-Universitat de Valencia (UV) and IFIC (UV-CSIC), 46100 Valencia, Spain*
[c] *Université de Lyon, Institut de Physique Nucléaire de Lyon, IN2P3-CNRS–UCBL, 4 rue Enrico Fermi, 69622 Villeurbanne, France*

A R T I C L E   I N F O

A B S T R A C T

We present the first full-fledged study of the flavor-exotic isoscalar $T_{bb}^- \equiv bb\bar{u}\bar{d}$ tetraquark with spin and parity $J^P = 1^+$. We report accurate solutions of the four-body problem in a quark model, characterizing the structure of the state as a function of the ratio M_Q/m_q of the heavy to light quark masses. For such a standard constituent model, T_{bb}^- lies approximately 150 MeV below the strong decay threshold $B^- \bar{B}^{*0}$ and 105 MeV below the electromagnetic decay threshold $B^- \bar{B}^0 \gamma$. We evaluate the lifetime of T_{bb}^-, identifying the promising decay modes where the tetraquark might be looked for in future experiments. Its total decay width is $\Gamma \approx 87 \times 10^{-15}$ GeV and therefore its lifetime $\tau \approx 7.6$ ps. The promising final states are $B^{*-} D^{*+} \ell^- \bar{\nu}_\ell$ and $\bar{B}^{*0} D^{*0} \ell^- \bar{\nu}_\ell$ among the semileptonic decays, and $B^{*-} D^{*+} D_s^{*-}$, $\bar{B}^{*0} D^{*0} D_s^{*-}$, and $B^{*-} D^{*+} \rho^-$ among the nonleptonic ones. The semileptonic decay to the isoscalar $J^P = 0^+$ tetraquark T_{bc}^0 is also relevant but it is not found to be dominant. There is a broad consensus about the existence of this tetraquark, and its detection will validate our understanding of the low-energy realizations of Quantum Chromodynamics (QCD) in the multiquark sector.

1. Introduction

Hadronic physics has been much stimulated during the last two decades by the experimental discovery of several new resonances in the hidden-charm sector, resonances that are hardly accommodated in the traditional quark-antiquark or three-quark picture [1]. These are the so-called XYZ mesons and LHCb pentaquarks, which belong to the class of "exotic hadrons", although they are not flavor exotics. After several years of studies, no definite conclusion has been drawn as to whether such non-flavor exotic states correspond to multiquark structures or to hadron-hadron molecules. A similar situation was encountered in the light scalar meson sector, where a multiquark picture was first introduced [2] as an attempt to explain the inverted mass spectrum (inverted in comparison to the simple quark-antiquark structure favored by the naive quark model) exhibited by the low-lying scalar mesons, some of which were later on suggested to be meson-meson molecules [3].

For years, the sector of flavor-exotic hadrons has been somewhat forgotten, as being less easily accessible than the hidden-flavor sector. However, already some decades ago, investigations on flavor-exotic multiquarks concluded that $\bar{q}\bar{q}$ four-quark configurations become more and more deeply bound when the mass ratio M_Q/m_q increases [4]. There is nowadays a broad theoretical consensus about the existence of such unconventional tetraquark configurations for which all strong decays are energetically forbidden. The most promising candidate is an isoscalar tetraquark with double beauty and $J^P = 1^+$ quantum numbers, which is stable against strong and electromagnetic decays. The same conclusion about the stability of this state has been reached in a wide variety of theoretical approaches [4–14]. A novel lattice QCD calculation [5] employing a non-relativistic formulation to simulate the bottom quark finds unambiguous signals for a strong-interaction-stable $(I)J^P = (0)1^+$ tetraquark, 189(10) MeV below the corresponding two-meson threshold, $\bar{B}\bar{B}^*$. The lattice QCD calculation of Ref. [6] come to the identical conclusion obtaining a binding energy of 143(34) MeV. With such binding, the tetraquark is stable also with respect to electromagnetic decays. In Ref. [7], the mass of the doubly-charm baryon Ξ_{cc}^{++}, discovered by the LHCb Collaboration [15], is used to calibrate the binding energy of a

QQ diquark. Assuming that the bb diquark binding energy in a T_{bb}^- tetraquark is the same as that of the cc diquark in the Ξ_{cc}^{++} baryon, the mass of the $(0)1^+$ doubly-bottom tetraquark is estimated to be 215 MeV below the strong decay threshold $\bar{B}\bar{B}^*$. In Ref. [8], the heavy-quark-symmetry mass relations linking heavy-light and doubly-heavy-light mesons and baryons are combined with leading-order corrections for finite heavy-quark mass, corresponding to hyperfine spin-dependent terms and kinetic energy shift that depends only on the light degrees of freedom. This leads to predict that the T_{bb}^- state is stable against strong decays. More specifically, using as input the masses of the doubly-bottom baryons (not yet experimentally measured) obtained by the model calculations of Ref. [7], Ref. [8] finds an axial-vector tetraquark bound by 121 MeV. In Ref. [9], the Schrödinger equation is solved with a potential extracted from a lattice QCD calculation for static heavy quarks, in a regime where the pion mass is $m_\pi \sim 340$ MeV, and again, evidence is found for a stable isoscalar doubly-bottom axial-vector tetraquark. When extrapolated to physical pion masses it has a binding energy of 90^{+43}_{-36} MeV. The robustness of these predictions is reinforced by detailed few-body calculations using phenomenological constituent models based on quark-quark Cornell-type interactions [10,11], which predict that the isoscalar axial-vector doubly-bottom tetraquark is strong- and electromagnetic-interaction stable with a binding energy ranging between 144–214 MeV for different realistic quark-quark potentials. Recent studies using a simple color-magnetic model have come to similar conclusions [12]. The QCD sum rule analysis of Ref. [13] also points to the possibility of a stable doubly-bottom isoscalar axial-vector tetraquark. Finally, the recent phenomenological analysis of Ref. [14] also presents evidence in favor of the existence of a stable T_{bb}^- state.

The compelling theoretical evidence for the existence of a T_{bb}^- tetraquark has led to preliminary studies of its lifetime and weak decay modes. In this context, Ref. [16] investigated the amplitudes and decay widths of doubly-heavy tetraquarks under the flavor SU(3) symmetry, deriving ratios between decay widths of different channels. Ref. [17] evaluated the semileptonic decay of the T_{bb}^- tetraquark to a scalar $bc\bar{u}\bar{d}$ tetraquark in the framework of QCD sum rules. In spite of the numerous model calculations existing in the literature (see Refs. [11,12] for a recent compendium) no comprehensive calculation of the spectroscopy, decay modes, and lifetime of this state has been obtained so far.

The purpose of this work is to present the first detailed study of the flavor-exotic T_{bb}^- tetraquark with $J^P = 1^+$ and isospin $I = 0$, reporting accurate solutions of the four-body problem, characterizing the structure of the state, evaluating its lifetime and identifying the promising decay modes where the tetraquark might be looked for. A striking result deals with the lifetime, which is found significantly longer than for single-b hadrons. With two b quarks, one expects either cooperating or conflicting interferences. Also, if one compares a typical meson decay mode $B \to D x$ and its tetraquark analog $T \to B D x$, there is a change in the overlap of the final D meson and the $c\bar{q}$ system provided by a spectator $\bar{q}$ and the c quark coming from one of the b quarks: the color factor and the spatial distribution are modified. There is also an obvious effect of the phase-space, which is known to be crucial in weak decays, for instance for β-unstable nuclei. While the Dx invariant mass is 5.3 GeV in $B \to Dx$ decay, it is about 4.6 GeV in $T \to BDx$, depending which sector of the Dalitz plot is reached. Altogether, it looks difficult to attempt a guesstimate of the lifetime before actually performing the calculation.

This paper is organized as follows. In Sec. 2, we present the masses and wave functions obtained from an accurate four-body calculation that makes use of a quark model. The calculation of

the dominant decay modes and of the lifetime is given in Sec. 3. Our conclusions are summarized in Sec. 4.

2. Tetraquark mass and wave function

We have studied the spectroscopy of doubly-heavy tetraquarks by two different numerical methods: a hyperspherical harmonic formalism and a generalized Gaussian variational (GGV) approach, both driving to the same results [10]. For its later application to the detailed study of the four-quark structure and weak decays, the GGV is more suited. Let us briefly discuss the main characteristics of the method. We shall denote the heavy quark coordinates by $\boldsymbol{r}_1$ and $\boldsymbol{r}_2$, and those of the light antiquarks by $\boldsymbol{r}_3$ and $\boldsymbol{r}_4$. The tetraquark wave function is taken to be a sum over all allowed channels with well-defined symmetry properties [18,19]:

$$\psi(\boldsymbol{x}, \boldsymbol{y}, \boldsymbol{z}) = \sum_{\kappa=1}^{6} \chi_\kappa^{csf} R_\kappa(\boldsymbol{x}, \boldsymbol{y}, \boldsymbol{z}), \tag{1}$$

where $\boldsymbol{x} = \boldsymbol{r}_1 - \boldsymbol{r}_2$, $\boldsymbol{y} = \boldsymbol{r}_3 - \boldsymbol{r}_4$ and $\boldsymbol{z} = (\boldsymbol{r}_1 + \boldsymbol{r}_2 - \boldsymbol{r}_3 - \boldsymbol{r}_4)/2$ are the Jacobi coordinates. χ_κ^{csf} are orthonormalized color-spin-flavor vectors and $R_\kappa(\boldsymbol{x}, \boldsymbol{y}, \boldsymbol{z})$ is the radial part of the wave function of the κth channel. In order to get the appropriate symmetry properties in configuration space, $R_\kappa(\boldsymbol{x}, \boldsymbol{y}, \boldsymbol{z})$ is expressed as the sum of four components,

$$R_\kappa(\boldsymbol{x}, \boldsymbol{y}, \boldsymbol{z}) = \sum_{n=1}^{4} w_\kappa^n R_\kappa^n(\boldsymbol{x}, \boldsymbol{y}, \boldsymbol{z}), \tag{2}$$

where $w_\kappa^n = \pm 1$. Finally, each $R_\kappa^n(\boldsymbol{x}, \boldsymbol{y}, \boldsymbol{z})$ is expanded in terms of N generalized Gaussians

$$\begin{aligned} R_\kappa^n(\boldsymbol{x}, \boldsymbol{y}, \boldsymbol{z}) = \sum_{i=1}^{N} \alpha_\kappa^i \exp\big[&- a_\kappa^i \boldsymbol{x}^2 - b_\kappa^i \boldsymbol{y}^2 - c_\kappa^i \boldsymbol{z}^2 \\ &- d_\kappa^i s_1(n) \boldsymbol{x} \cdot \boldsymbol{y} - e_\kappa^i s_2(n) \boldsymbol{x} \cdot \boldsymbol{z} - f_\kappa^i s_3(n) \boldsymbol{y} \cdot \boldsymbol{z} \big], \end{aligned} \tag{3}$$

where $s_i(n)$ are equal to ± 1 to guarantee the symmetry properties of the radial function and $\alpha_\kappa^i, a_\kappa^i, \cdots, f_\kappa^i$ are the variational parameters. The latter are determined by minimizing the intrinsic energy of the tetraquark. We follow closely the developments of Refs. [18, 19], where further technical details can be found about the wave function and the minimization procedure.

A four-quark state is stable under the strong interaction if its mass, M_T (from now on, T often abbreviates T_{QQ}), lies below all allowed two-meson decay thresholds. Thus, one can define the difference between the mass of the tetraquark and that of the lowest two-meson threshold, namely:

$$\Delta E = M_T - (M_1 + M_2), \tag{4}$$

where M_1 and M_2 are the masses of the mesons constituting the threshold. When $\Delta E < 0$, all fall-apart decays are forbidden and, therefore, the state is stable under strong interactions. When $\Delta E \geq 0$ one has to examine whether it is a resonance or an artifact of the discretization of the continuum by the variational method, and this requires dedicated techniques such as real [20] or complex scaling [21], which are beyond the scope of this note. We therefore concentrate on $\Delta E < 0$. Another quantity of interest is the root-mean-square (r.m.s.) radius of the tetraquark, X_T, given by [10]:

Table 1
Relevant meson masses (in MeV) and r.m.s. radii (in fm) predicted by the AL1 model for the strong, electromagnetic and weak decay thresholds of the $J^P = 1^+$ T_{bb}^- tetraquark.

	Meson	M	r.m.s.	Meson	M	r.m.s
$J = 0$	$\bar{B}$	5293	0.145	K	491	0.283
	D	1862	0.216	π	138	0.298
	D_s	1962	0.213	η_c	3005	0.181
$J = 1$	$\bar{B}^*$	5350	0.153	K^*	903	0.389
	D^*	2016	0.248	ρ	770	0.460
	D_s^*	2102	0.243	J/Ψ	3101	0.199

$$X_T = \left[\frac{\sum_{i=1}^4 m_i \langle (\boldsymbol{r}_i - \boldsymbol{R})^2 \rangle}{\sum_{i=1}^4 m_i} \right]^{1/2}, \tag{5}$$

where $\boldsymbol{R}$ is the center-of-mass coordinate, and m_i are the quark masses M_Q or m_q.

Determining whether stability is reached in this model, i.e., $\Delta E < 0$, requires a simultaneous and consistent calculation of the meson masses M_1 and M_2 entering the threshold, and of the tetraquark configurations. For this purpose, we have adopted the so-called AL1 model by Semay and Silvestre-Brac [22], already used in a number of exploratory studies of multiquark systems, for instance in our recent investigation of the hidden-charm pentaquark sector $\bar{c}cqqq$ [23] or doubly-heavy baryons and tetraquarks [11]. It includes a standard Coulomb-plus-linear central potential, supplemented by a smeared version of the chromomagnetic interaction,

$$V(r) = -\frac{3}{16} \tilde{\lambda}_i . \tilde{\lambda}_j \left[\lambda r - \frac{\kappa}{r} - \Lambda + \frac{V_{SS}(r)}{m_i m_j} \boldsymbol{\sigma}_i \cdot \boldsymbol{\sigma}_j \right],$$

$$V_{SS}(r) = \frac{2 \pi \kappa'}{3 \pi^{3/2} r_0^3} \exp\left(-\frac{r^2}{r_0^2}\right), \quad r_0 = A \left(\frac{2 m_i m_j}{m_i + m_j}\right)^{-B}, \tag{6}$$

where $\lambda = 0.1653$ GeV^2, $\Lambda = 0.8321$ GeV, $\kappa = 0.5069$, $\kappa' = 1.8609$, $A = 1.6553$ GeV^{B-1}, $B = 0.2204$, $m_u = m_d = 0.315$ GeV, $m_s = 0.577$ GeV, $m_c = 1.836$ GeV and $m_b = 5.227$ GeV. Here, $\tilde{\lambda}_i . \tilde{\lambda}_j$ is a color factor, suitably modified for the quark-antiquark pairs. We disregard the small three-body term of this model used in [22] to fine-tune the baryon masses vs. the meson masses. Note that the smearing parameter of the spin-spin term is adapted to the masses involved in the quark-quark or quark-antiquark pairs. It is worth to emphasize that the parameters of the AL1 potential are constrained in a simultaneous fit of 36 well-established meson states and 53 baryons, with a remarkable agreement with data, as seen in Table 2 of Ref. [22].

The meson masses of the threshold in this model are given in Table 1, together with the masses of other mesons that will be involved in the weak decays discussed in Sec. 3. Also shown is the quark-antiquark r.m.s. radius.

One can now study the stability of the $J^P = 1^+$ T_{bb}^- isoscalar state. In the GGV method, if a state is unbound, one observes a slow decrease of its mass toward $M_1 + M_2$ as N, the number of terms in Eq. (3), increases. It turns out to be useful to also look at the content of the variational wave function, which comes very close to 100% in a color singlet-singlet channel in the physical basis [18]. On the other hand, if a variational state converges to a bound state as N increases, it includes sizable hidden-color components even for low N. We show in Table 2 the results for the T_{QQ} tetraquark for different masses of the heavy quark, M_Q. In the first line we give the results for the standard mass value of the bottom quark used in the AL1 model, for which we get a binding energy of 151 MeV. We have scrutinized the structure of the T_{QQ} state. For each particular value of M_Q we have evaluated the lowest strong-decay threshold, $M_1 + M_2$, the energy of the four-quark

Table 2
Properties of the T_{QQ} tetraquark as a function of the mass of the heavy quark M_Q for the AL1 model. Energies and masses are in MeV and distances in fm. For $\Delta E > 0$, the probabilities and average distances are just an indication that the variational calculation will likely not converge toward a bound state.

| M_Q	$M_1 + M_2$	$M_{T_{QQ}}$	ΔE	$P[|\bar{6}\bar{6}\rangle]$	$P[|\bar{3}3\rangle]$	$P[|11\rangle]$	$P[|88\rangle]$	P_{MM^*}	$P_{M^*M^*}$	$\langle x^2 \rangle^{1/2}$	$\langle y^2 \rangle^{1/2}$	$\langle z^2 \rangle^{1/2}$	$X_{T_{QQ}}$
5227	10644	10493	−151	0.033	0.967	0.344	0.656	0.561	0.439	0.334	0.784	0.544	0.226
4549	9290	9163	−126	0.045	0.955	0.348	0.652	0.597	0.403	0.362	0.791	0.544	0.242
3871	7936	7835	−100	0.070	0.930	0.357	0.643	0.646	0.354	0.411	0.806	0.541	0.268
3193	6582	6511	−71	0.115	0.885	0.372	0.628	0.730	0.270	0.475	0.833	0.536	0.301
2515	5230	5189	−41	0.222	0.778	0.407	0.593	0.795	0.205	0.621	0.919	0.523	0.369
1836	3878	3865	−13	0.421	0.579	0.474	0.526	0.880	0.120	0.966	1.181	0.499	0.530
1158	2534	2552	> 0	0.667	0.333	0.556	0.444	1.000	0.000	$\gg 1$	$\gg 1$	0.470	$\gg 1$
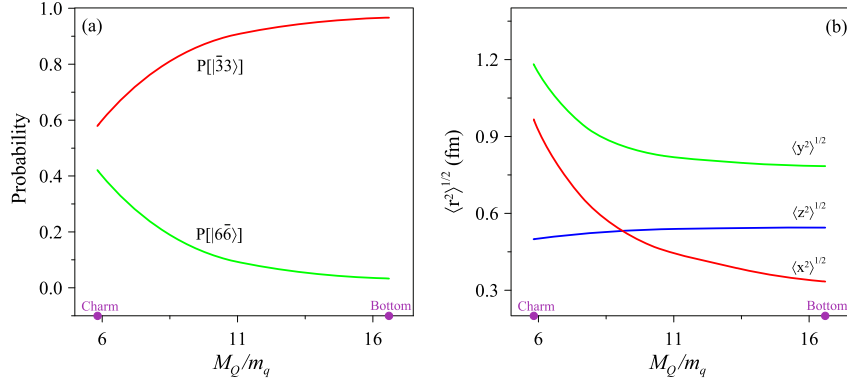
Fig. 1. (a) Probability of the $\bar{3}3$ and $6\bar{6}$ components of the T_{QQ} color wave function as a function of M_Q/m_q. (b) Average distances $\langle x^2 \rangle^{1/2}$, $\langle y^2 \rangle^{1/2}$ and $\langle z^2 \rangle^{1/2}$ as a function of M_Q/m_q.

state, $M_{T_{QQ}}$, and the corresponding binding energy $B = -\Delta E$. We have calculated the probability of the $\bar{3}3$, $P[|\bar{3}3\rangle]$, and $6\bar{6}$, $P[|6\bar{6}\rangle]$, color components. By using the recoupling techniques derived in Ref. [18] we have also evaluated the probability of the 11, $P[|11\rangle]$, and 88, $P[|88\rangle]$, color components. Afterwards, we have expanded the wave function in terms of physical states evaluating the probability of the pseudoscalar-vector, P_{MM^*}, and vector-vector, $P_{M^*M^*}$, two-meson physical states. Finally we have calculated the average distance between the two heavy quarks, $\langle x^2 \rangle^{1/2}$, between the two light quarks, $\langle y^2 \rangle^{1/2}$, between a heavy and a light quarks, $\langle z^2 \rangle^{1/2}$, and the four-quark r.m.s. radius, $X_{T_{QQ}}$.

As shown in Table 2 the binding energy of the T_{QQ} tetraquark increases with increasing M_Q/m_q as predicted in Ref. [4] and recently rediscovered in Refs. [7,8]. Close to $\Delta E = 0$ the system behaves like a simple meson-meson molecule, with a large probability in a single meson-meson component, the pseudoscalar-vector channel. The T_{QQ} starts to be bound around the mass of the charm quark used by the AL1 model, $m_c = 1836$ MeV [24]. Such small binding is due to a cooperative effect between the chromo-electric and chromomagnetic pieces in the interacting potential. Hence, the T_{cc} tetraquark is unbound when the spin-spin interaction is switched off. The $\tilde{\lambda}_i.\tilde{\lambda}_j$ contribution of Eq. (6), with a pairwise potential due to color-octet exchange, induces mixing between $\bar{3}3$ and $6\bar{6}$ color states in the $QQ - \bar{q}\bar{q}$ basis. The ground state of the $QQ\bar{u}\bar{d}$ with $J^P = 1^+$ has its dominant component with color $\bar{3}3$, and spin $\{1, 0\}$ in the $QQ - \bar{u}\bar{d}$ basis. The main admixture consists of $6\bar{6}$ with spin $\{0, 1\}$ and a symmetric orbital wave function. Thus, for M_Q/m_q close to the charm sector, the binding requires both the color mixing of $\bar{3}3$ with $6\bar{6}$, and the spin-spin interaction [11,25]. In the most advanced calculations of Ref. [25], it was acknowledged that a pure additive interaction will not bind $cc\bar{q}\bar{q}$, on the sole basis that this tetraquark configuration benefits from the strong cc chromoelectric attraction that is absent in the $Q\bar{q} + Q\bar{q}$ threshold. In the case where $\bar{q}\bar{q} = \bar{u}\bar{d}$, however, there is in addition a favorable chromomagnetic interaction in the tetraquark, while the threshold experiences only heavy-light spin-spin interaction, whose strength is suppressed by a factor m_q/M_Q.

When the ratio M_Q/m_q increases, the probability of the $6\bar{6}$ color component diminishes in such a way that the system does not behave any more like a simple meson-meson molecule. The probability of the $6\bar{6}$ component in a compact $QQ\bar{q}\bar{q}$ tetraquark tends to zero for $M_Q \to \infty$. Therefore, heavy-light compact bound states would be almost a pure $\bar{3}3$ singlet color state and not a single colorless meson-meson 11 molecule, as shown in Table 2. Such compact states with two-body colored components can be expanded as the mixture of several physical meson-meson channels [10,26], and thus they can be also studied as an involved coupled-channel problem of physical meson-meson states [27].

We have shown these results in Fig. 1. In the panel (a), we see how the probability of the $6\bar{6}$ color component tends to zero for $M_Q \to \infty$. On the other hand, we can also see the failure of treating heavy-light tetraquarks as a single $\bar{3}3$ color state for charm-light or charm-strange doubly-heavy tetraquarks. In the panel (b) of Fig. 1 we show the expectation value of the different Jacobi coordinates over the tetraquark wave function, i.e., the average distance between the different constituents of the tetraquark [10]. One can see how when the binding increases, i.e. M_Q/m_q augments, the average distance between the two heavy quarks, $\langle x^2 \rangle^{1/2}$, diminishes rapidly, while that of the two light quarks, $\langle y^2 \rangle^{1/2}$, although diminishing, remains larger. The heavy-to-light quark distance, $\langle z^2 \rangle^{1/2}$, stays almost constant for any value of M_Q/m_q. It is also worth noting how the tetraquark becomes compact in the bottom sector. As can be seen from Tables 1 and 2, for deep binding, $X_{T_{QQ}}/\text{r.m.s.}(M_1 + M_2) = 0.226/0.298 < 1$, the tetraquark is smaller than the two mesons of the threshold while close to $\Delta E = 0$, $X_{T_{QQ}}/\text{r.m.s.}(M_1 + M_2) = 0.530/0.464 > 1$, it becomes larger, being very likely the break down into two mesons. Thus, in the heavy-quark limit, the lowest lying tetraquark configuration resembles the Helium atom [8,28], a factorized system with separate dynamics for the compact color $\bar{3}$ QQ *kernel* and for the light quarks bound to the stationary color 3 state, to construct a $QQ\bar{q}\bar{q}$ color singlet. As mentioned above, this result is less pronounced for other systems like charm-light ($cc\bar{q}\bar{q}$) or charm-strange ($cs\bar{q}\bar{q}$) doubly-heavy tetraquarks. On the basis of the results shown in Table 2, the schematic evolution of the T_{QQ} state as a function of the ratio M_Q/m_q, in other words, from deep binding to a close-to-threshold meson-meson state, is shown in Fig. 2 [29].

3. Tetraquark lifetime and decay modes

The double beauty T_{bb}^- isoscalar tetraquark with $J^P = 1^+$ is stable with respect to strong- and electromagnetic interactions [4–14], and thus it decays weakly. We have studied the semileptonic and nonleptonic decays of T_{bb}^- following closely the method developed in Ref. [30]. We present here the results for the most favorable final states where T_{bb}^- might be looked for. The remaining channels and a detailed discussion of the technicalities will be presented elsewhere [31].

Among the semileptonic decays one can distinguish between processes with final states with a single meson, see panel (a) of Fig. 3, or those with two mesons, panel (b) of Fig. 3. The first case, $T_{bb}^- \to \bar{B}^0 \ell^- \bar{\nu}_\ell$, involves a $b\bar{u} \to W^- \to \ell^- \bar{\nu}_\ell$ transition that at tree level is described by the operator

$$-iV_{ub}\frac{G_F}{\sqrt{2}}\overline{\Psi}_u(0)\gamma^\mu(1 - \gamma_5)\Psi_b(0)\,\overline{\Psi}_\ell(0)\gamma_\mu(1 - \gamma_5)\Psi_{\nu_\ell}(0),\quad (7)$$
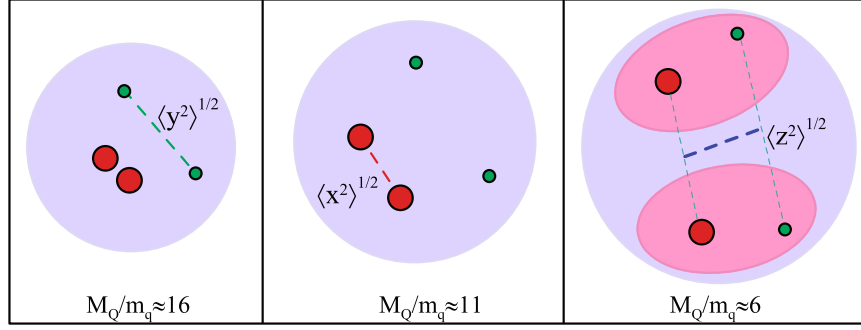
Fig. 2. From left to right, schematic evolution of a T_{QQ} state as the heavy-quark mass decreases and, thus, the separation between the heavy quarks increases. The separation between the light quarks starts to augment close to threshold and the separation between the heavy and the light quarks remains almost constant. The last scenario, $M_Q/m_q \approx 6$ is close to threshold, compatible with a T_{QQ} molecule or two heavy-light mesons.
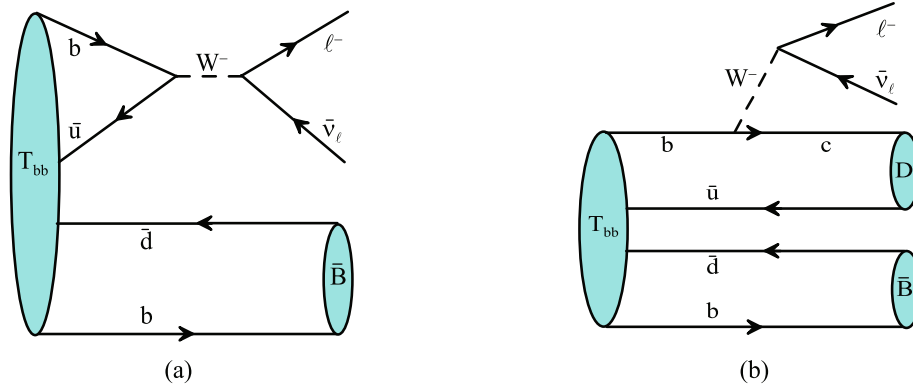

Fig. 3. Representative diagrams for semileptonic decays of the T_{bb} tetraquark: (a) Final state with a single meson. (b) Final state with two mesons.

where Ψ_f is a quark field of a definite flavor f, G_F is the Fermi coupling constant and V_{ub} is the Cabibbo-Kobayashi-Maskawa (CKM) matrix element. The decay width is given by

$$\Gamma = \frac{1}{2m_T} \iiint \frac{d\boldsymbol{P}_B}{(2\pi)^3 2E_B} \frac{d\boldsymbol{p}_\ell}{(2\pi)^3 2E_\ell} \frac{d\boldsymbol{p}_{\nu_\ell}}{(2\pi)^3 2E_{\nu_\ell}}$$
$$\times (2\pi)^4 \delta^{(4)}(P_T - P_B - p_\ell - p_{\nu_\ell})$$
$$\times |V_{ub}|^2 \frac{G_F^2}{2} \mathcal{L}^{\alpha\beta}(p_\ell, p_{\nu_\ell}) \mathcal{W}_{\alpha\beta}(P_T, P_B), \qquad (8)$$

where the lepton[1] and hadron tensors are given by,

$$\mathcal{L}^{\alpha\beta} = 8(p_\ell^\alpha p_{\nu_\ell}^\beta + p_\ell^\beta p_{\nu_\ell}^\alpha - g^{\alpha\beta} p_\ell \cdot p_{\nu_\ell} \pm i\epsilon^{\alpha\beta\rho\lambda} p_{l\rho} p_{\nu_\ell\lambda}), \quad (9)$$

$$\mathcal{W}_{\alpha\beta} = \frac{1}{2J_T + 1} \sum_{\lambda,\lambda'} h_\alpha^{T \to B} (h_\beta^{T \to B})^* \qquad (10)$$

$$h_\alpha^{T \to B} = \langle B, \lambda' \, \boldsymbol{P}_B | \overline{\Psi}_u(0) \gamma_\alpha (1 - \gamma_5) \Psi_b(0) | T, \lambda \, \boldsymbol{0} \rangle, \qquad (11)$$

where p_i is the four-momentum of the particle i, J_T stands for the spin of the tetraquark, $|M, \lambda' \, \boldsymbol{P}_M\rangle$ represents the state of an M meson with three momentum $\boldsymbol{P}_M$ and spin projection in the meson center of mass λ', and $|T, \lambda \, \boldsymbol{0}\rangle$ is the state of the tetraquark at rest. $\epsilon^{\alpha\beta\rho\lambda}$ is the fully antisymmetric tensor for which we take the convention $\epsilon^{0123} = +1$ and $g^{\alpha\alpha} = (1, -1, -1, -1)$. Equation (8) can be further simplified

$$\Gamma = |V_{ub}|^2 \frac{G_F^2}{2^4 \pi^3 m_T}$$

$$\times \iint dE_B dE_\ell \, \Theta(m_T - E_B - E_\ell) \, \Theta(1 - |\cos\theta_\ell^0|)$$
$$\times \tilde{\mathcal{L}}^{\alpha\beta} \, \mathcal{W}_{\alpha\beta}(P_T, \tilde{P}_B), \qquad (12)$$

with $\tilde{P}_B^\mu = (E_B, 0, 0, |\boldsymbol{P}_B|)$ and

$$\cos\theta_\ell^0 = \frac{(m_T - E_B - E_\ell)^2 - |\boldsymbol{P}_B|^2 - |\boldsymbol{p}_\ell|^2}{2|\boldsymbol{P}_B||\boldsymbol{p}_\ell|}. \qquad (13)$$

In (12), since all the dependence on φ_ℓ appears only in the lepton tensor, we have defined

$$\tilde{\mathcal{L}}^{\alpha\beta} = \frac{1}{16\pi} \int d\varphi_\ell \, \mathcal{L}^{\alpha\beta}. \qquad (14)$$

The matrix element (11) appearing in the hadron tensor can be expanded as,

$$h_\rho^{T \to B}$$
$$= 4\sqrt{m_T E_B} \iint d\boldsymbol{p}_x d\boldsymbol{p}_z$$
$$\times \sum_{\substack{\alpha_1,\alpha_2 \\ \alpha_3,\alpha_4}} \left[\hat{\phi}_{\alpha_2,\alpha_4}^{(B,\lambda')} \left(\frac{m_b}{m_b + m_u} \boldsymbol{P}_B + \boldsymbol{p}_x - \frac{1}{2} \boldsymbol{p}_z \right) \right]^*$$
$$\times \hat{\phi}_{\substack{\alpha_1,\alpha_2 \\ \alpha_3,\alpha_4}}^{(T,\lambda)} (\boldsymbol{p}_x, -\boldsymbol{p}_x - \boldsymbol{P}_B, \boldsymbol{p}_z)$$
$$\times \frac{(-1)^{1/2 - s_3}}{2\sqrt{E_u E_b}} \bar{v}_u^{s_3} \left(-\boldsymbol{P}_B - \boldsymbol{p}_x - \frac{1}{2} \boldsymbol{p}_z \right) \gamma_\rho (1 - \gamma_5)$$
$$\times u_b^{s_1} \left(\boldsymbol{p}_x + \frac{1}{2} \boldsymbol{p}_z \right) \delta_{c_1 c_3} \delta_{f_1 b} \delta_{f_3 u}, \qquad (15)$$
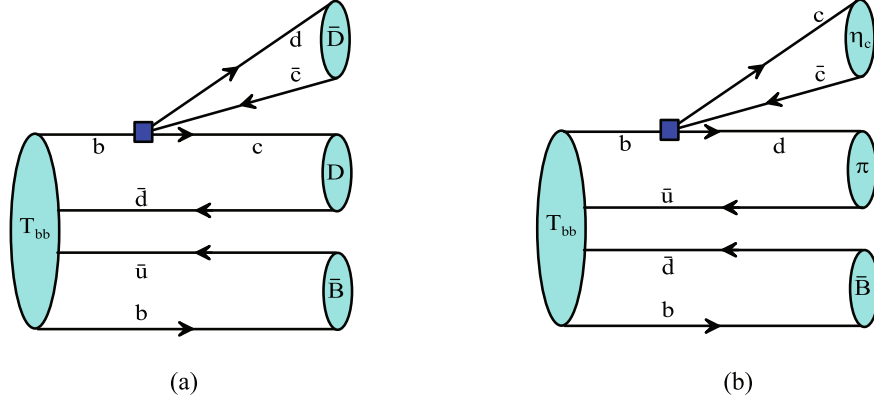
Fig. 4. Representative diagrams for nonleptonic decays of the T_{bb} tetraquark: (a) Final state with only open flavor mesons. (b) Final state with hidden flavor mesons. The blue box represents a four-quark effective vertex containing the contribution of the W boson and radiative corrections as seen in Eq. (21).

where $\hat{\phi}$ is the Fourier transform of the radial wave function, obtained in Sec. 2 using the AL1 constituent model, and α_i represents the quantum numbers of spin s_i, flavor f_i and color c_i ($\alpha_i \equiv (s_i, f_i, c_i)$) of a quark or an antiquark.

For the second class of semileptonic decays represented diagrammatically in panel (b) of Fig. 3, with a $b \to c$ transition at the quark level, the operator is given by

$$-i V_{cb} \frac{G_F}{\sqrt{2}} \overline{\Psi}_c(0) \gamma^\mu (1-\gamma_5) \Psi_b(0) \, \overline{\Psi}_\ell(0) \gamma_\mu (1-\gamma_5) \Psi_{\nu_\ell}(0), \quad (16)$$

and the decay width can be expressed as

$$\Gamma = |V_{cb}|^2 \frac{G_F^2}{2^7 \pi^5 m_T} \iiiint |\boldsymbol{P}_B| dE_B d\cos\theta_D |\boldsymbol{P}_D| dE_D$$

$$\times \frac{1}{|\tilde{\boldsymbol{P}}_B + \boldsymbol{P}_D|} dE_\ell \, \Theta(1 - |\cos\theta_\ell^0|)$$

$$\times \Theta(m_T - E_B - E_D - E_\ell) \, \tilde{\mathcal{L}}^{\alpha\beta} \mathcal{W}_{\alpha\beta}(P_T, \hat{P}_B, \hat{P}_D), \quad (17)$$

where $\hat{P}_B = \mathcal{R}' \tilde{P}_B$ and $\hat{P}_D = \mathcal{R}' P_D$, where $\mathcal{R}'$ is a rotation that, for a fixed $\boldsymbol{P}_D$, takes $\tilde{\boldsymbol{P}}_B + \boldsymbol{P}_D \to (0, 0, |\tilde{\boldsymbol{P}}_B + \boldsymbol{P}_D|)$. In this case,

$$\cos\theta_\ell^0 = \frac{(m_T - E_B - E_D - E_\ell)^2 - |\tilde{\boldsymbol{P}}_B + \boldsymbol{P}_D|^2 - |\boldsymbol{p}_\ell|^2}{2 |\tilde{\boldsymbol{P}}_B + \boldsymbol{P}_D| |\boldsymbol{p}_\ell|}. \quad (18)$$

The matrix element appearing in the hadron tensor

$$h_\rho^{T \to M_1 M_2} =$$
$$\langle M_1, \lambda'' \, \boldsymbol{P}_1 | \langle M_2, \lambda' \, \boldsymbol{P}_2 | \overline{\Psi}_c(0) \gamma_\rho (1-\gamma_5) \Psi_b(0) | T, \lambda \, \boldsymbol{0} \rangle, \quad (19)$$

here written for a $T \to BD$ transition (for other cases, the changes are obvious), can be expressed as,

$$h_\rho^{T \to BD} = 4 (2\pi)^{3/2} \sqrt{2 m_T E_B E_D} \sum_{\substack{\alpha_2, \alpha_3 \\ \alpha_4, \alpha_5}} \iint d\boldsymbol{p}_x d\boldsymbol{p}_z$$

$$\times \left[\hat{\phi}_{\alpha_5, \alpha_3}^{(D, \lambda'')} \left(-\frac{m_u}{m_c + m_u} \boldsymbol{P}_D - \boldsymbol{P}_B - \boldsymbol{p}_x - \frac{1}{2} \boldsymbol{p}_z \right) \right]^*$$

$$\times \left[\hat{\phi}_{\alpha_2, \alpha_4}^{(B, \lambda')} \left(\frac{m_b}{m_b + m_u} \boldsymbol{P}_B + \boldsymbol{p}_x - \frac{1}{2} \boldsymbol{p}_z \right) \right]^*$$

$$\times \sum_{\alpha_1} \hat{\phi}_{\substack{\alpha_1, \alpha_2 \\ \alpha_3, \alpha_4}}^{(T, \lambda)} (\boldsymbol{p}_x, -\boldsymbol{p}_x - \boldsymbol{P}_B, \boldsymbol{p}_z)$$

$$\times \frac{1}{2\sqrt{E_c E_b}} \bar{u}_c^{s_5} \left(\boldsymbol{P}_D + \boldsymbol{P}_B + \boldsymbol{p}_x + \frac{1}{2} \boldsymbol{p}_z \right) \gamma_\rho (1-\gamma_5)$$

$$\times u_b^{s_1} \left(\boldsymbol{p}_x + \frac{1}{2} \boldsymbol{p}_z \right) \delta_{c_1 c_5} \delta_{f_1 b} \delta_{f_5 c}. \quad (20)$$

Obviously B could also be a B^* and D a D^*. If we have a $b \to u$ quark transition, one has to change $V_{cb} \to V_{ub}$ and the meson in the final state (apart from $B(B^*)$) would be a nonstrange meson with $u\bar{u}$ or $u\bar{d}$ composition.

We evaluate now the width of the nonleptonic decays $T_{bb}^- \to B^- M_1 M_2$ or $\bar{B}^0 M_1' M_2'$ represented diagrammatically in Fig. 4. These decay modes involve a transition $b \to c, u$ at the quark level and they are governed, neglecting penguin operators, by the effective Hamiltonian [32–34]

$$H_{\text{eff}} = \frac{G_F}{\sqrt{2}} \left\{ V_{cb} \left[c_1(\mu) Q_1^{cb} + c_2(\mu) Q_2^{cb} \right] \right.$$

$$\left. + V_{ub} \left[c_1(\mu) Q_1^{ub} + c_2(\mu) Q_2^{ub} \right] + \text{h.c.} \right\}, \quad (21)$$

where c_1, c_2 are scale–dependent Wilson coefficients, and Q_1^{ib}, Q_2^{ib}, $i = u, c$, are local four-quark operators of the current-current type given by

$$Q_1^{ib} = \overline{\Psi}_i(0) \gamma_\mu (1-\gamma_5) \Psi_b(0)$$

$$\times \left[V_{ud}^* \overline{\Psi}_d(0) \gamma^\mu (1-\gamma_5) \Psi_u(0) + V_{us}^* \overline{\Psi}_s(0) \gamma^\mu (1-\gamma_5) \Psi_u(0) \right.$$

$$\left. + V_{cd}^* \overline{\Psi}_d(0) \gamma^\mu (1-\gamma_5) \Psi_c(0) + V_{cs}^* \overline{\Psi}_s(0) \gamma^\mu (1-\gamma_5) \Psi_c(0) \right], \quad (22)$$

$$Q_2^{ib} = \overline{\Psi}_d(0) \gamma_\mu (1-\gamma_5) \Psi_b(0)$$

$$\times \left[V_{ud}^* \overline{\Psi}_i(0) \gamma^\mu (1-\gamma_5) \Psi_u(0) + V_{cd}^* \overline{\Psi}_i(0) \gamma^\mu (1-\gamma_5) \Psi_c(0) \right]$$

$$+ \overline{\Psi}_s(0) \gamma_\mu (1-\gamma_5) \Psi_b(0)$$

$$\times \left[V_{us}^* \overline{\Psi}_i(0) \gamma^\mu (1-\gamma_5) \Psi_u(0) + V_{cs}^* \overline{\Psi}_i(0) \gamma^\mu (1-\gamma_5) \Psi_c(0) \right], \quad (23)$$

where the different V_{jk} are CKM matrix elements.

We work in the factorization approximation which amounts to evaluate the hadron matrix elements of the effective Hamiltonian as a product of two quark-current matrix elements: one is the matrix element for the $T_{bb} \to B M_1$ transition, and the other accounts for the transition from vacuum to the other final meson M_2, see Fig. 4. The latter coupling is governed by the corresponding meson decay constant. When writing the factorization amplitude, the relevant coefficients of the effective Hamiltonian (21) are the combinations,

Table 3
Meson decay constants, in GeV, used in this work.

f_{π^-}	f_{π^0}	f_{ρ^-,ρ^0}	f_{D^+}	$f_{D^{*+}}$	$f_{D_s^+}$	$f_{D_s^{*+}}$
0.1307 [35]	0.130 [35]	0.210 [33]	0.2226 [36]	0.245 [37]	0.294 [35]	0.272 [37]

$$a_1(\mu) = c_1(\mu) + \frac{1}{N_C}c_2(\mu) \qquad a_2(\mu) = c_2(\mu) + \frac{1}{N_C}c_1(\mu), \quad (24)$$

with $N_C = 3$ the number of colors. The energy scale μ appropriate in this case is $\mu \simeq m_b$ and the values for a_1 and a_2 that we use are [33]:

$$a_1 = 1.14 \qquad a_2 = -0.20. \quad (25)$$

Note that the W-exchange diagrams, that play an important role in the decay of charm, are suppressed in the decay of b since they are proportional to a_2. The total decay width is given as

$$\Gamma = \frac{1}{2m_T}\iiint \frac{d\boldsymbol{P}_B}{(2\pi)^3 2E_B}\frac{d\boldsymbol{P}_1}{(2\pi)^3 2E_1}\frac{d\boldsymbol{P}_2}{(2\pi)^3 2E_2}$$
$$\times (2\pi)^4 \delta^{(4)}(P_T - P_B - P_1 - P_2)$$
$$\times \frac{G_F^2}{2}\frac{1}{2J_T + 1}\sum_{\substack{\lambda_T,\lambda_B \\ \lambda_1,\lambda_2}}|\mathcal{M}_{\lambda_T\lambda_B\lambda_1\lambda_2}(P_T, P_B, P_1, P_2)|^2. \quad (26)$$

Using invariance arguments as in the semileptonic decay case one finds,

$$\Gamma = \frac{G_F^2}{2^7\pi^3 m_T}\iint dE_B dE_1$$
$$\times \Theta(1 - |\cos\theta_1^0|)\,\Theta(m_T - E_B - E_1 - M_2)$$
$$\times \frac{1}{2J_T + 1}\sum_{\substack{\lambda_T,\lambda_B \\ \lambda_1,\lambda_2}}\left|\mathcal{M}_{\lambda_T\lambda_B\lambda_1\lambda_2}(P_T, \tilde{P}_B, \hat{P}_1, \hat{P}_2)\right|^2, \quad (27)$$

where

$$\cos\theta_1^0 = \frac{(m_T - E_B - E_1)^2 - M_2^2 - |\boldsymbol{P}_B|^2 - |\boldsymbol{P}_1|^2}{2|\boldsymbol{P}_B||\boldsymbol{P}_1|}, \quad (28)$$

and $\mathcal{M}$ involves the product of a hadron matrix element such as Eq. (19) and meson decay constants that are taken from experiment or lattice data. For instance, for a $T_{bb} \to B^- D^+ D^-$ decay, one has that

$$\mathcal{M} = V_{cb}V_{cd}^* a_1 h_\alpha^{T\to B^-D^+} i f_{D^-} P_{D^-}^\alpha. \quad (29)$$

In particular, for the decays presented in Table 6, we have used the meson decay constants listed in Table 3.

For the sake of completeness we have also evaluated the decay of the $J^P = 1^+$ T_{bb}^- isoscalar tetraquark into the $J^P = 0^+$ T_{bc}^0 isoscalar tetraquark, decay depicted in Fig. 5. The mass of the $J^P = 0^+$ $bc\bar{u}\bar{d}$ isoscalar state has been estimated in Ref. [7] where the authors obtain a central value 11 MeV below the $\bar{B}D$ threshold, although it is cautioned that the precision of the calculation is not sufficient to determine whether the tetraquark is actually above or below this threshold. A systematic study of exotic $QQ'\bar{q}\bar{q}$ four-quark states containing distinguishable heavy flavors, b and c, has been recently performed with the AL1 model in Ref. [38]. The $J^P = 0^+$ isoscalar state was found to be strong and electromagnetic-interaction stable with a binding energy of around 23 MeV. Other independent calculations made in different frameworks arrive to similar conclusions. Among them, it is important to emphasize the lattice QCD results of Ref. [39] where
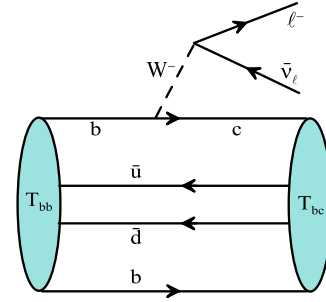
Fig. 5. Representative diagram for the semileptonic decay of the T_{bb} $J^P = 1^+$ tetraquark to the T_{bc} $J^P = 0^+$ tetraquark.

Table 4
Decay widths, in units of 10^{-15} GeV, for processes described by Fig. 3(a).

Final state	Γ [10^{-15} GeV]
$\bar{B}^{*0} e^- \bar{\nu}_e$	0.0365 ± 0.0004
$\bar{B}^0 e^- \bar{\nu}_e$	0.0394 ± 0.0006
$\bar{B}^{*0} \mu^- \bar{\nu}_\mu$	0.0355 ± 0.0004
$\bar{B}^0 \mu^- \bar{\nu}_\mu$	0.0396 ± 0.0006
$\bar{B}^{*0} \tau^- \bar{\nu}_\tau$	0.0355 ± 0.0004
$\bar{B}^0 \tau^- \bar{\nu}_\tau$	0.0396 ± 0.0006

it is found evidence for the existence of a strong-interaction-stable $(I)J^P = (0)1^+$ $bc\bar{u}\bar{d}$ four-quark state with a mass in the range of 15 to 61 MeV below the $D\bar{B}^*$ threshold. The decay width in this case is given by (12), changing the final B meson by the T_{bc}^0 tetraquark and V_{ub} by V_{cb}, while the corresponding hadronic matrix element is

$$h_\rho^{T\to T_{bc}} = 2\sqrt{2m_T E_{T_{bc}}}\sum_{\substack{\alpha_2,\alpha_3 \\ \alpha_4,\alpha_5}}\iiint d\boldsymbol{p}_x d\boldsymbol{p}_y d\boldsymbol{p}_z$$
$$\times \left[\hat{\phi}^{(T_{bc},\lambda')}_{\substack{\alpha_2,\alpha_5 \\ \alpha_3,\alpha_4}}\left(-\boldsymbol{p}_x - \frac{m_b - m_c}{2(m_b + m_c)}\boldsymbol{p}_z - \frac{m_b}{m_b + m_c}\boldsymbol{P}_{T_{bc}}, \boldsymbol{p}_y, \right.\right.$$
$$\left.\boldsymbol{p}_z + \frac{2m_u}{m_b + m_c + 2m_u}\boldsymbol{P}_{T_{bc}}\right)\Bigg]^*$$
$$\times \sum_{\alpha_1}\hat{\phi}^{(T,\lambda)}_{\substack{\alpha_1,\alpha_2 \\ \alpha_3,\alpha_4}}(\boldsymbol{p}_x, \boldsymbol{p}_y, \boldsymbol{p}_z)\frac{1}{2\sqrt{E_c E_b}}\bar{u}_c^{s_5}\left(\boldsymbol{P}_{T_{bc}} + \boldsymbol{p}_x + \frac{1}{2}\boldsymbol{p}_z\right)$$
$$\times \gamma_\rho(1 - \gamma_5)u_b^{s_1}\left(\boldsymbol{p}_x + \frac{1}{2}\boldsymbol{p}_z\right)\delta_{c_1 c_5}\delta_{f_1 b}\delta_{f_5 c}. \quad (30)$$

Let us now comment on the results. Some aspects could have been anticipated, and are verified. For instance, for the $T \to B^{(*)}$ semileptonic decays depicted in Fig. 3(a), and due to the large phase space available in all cases, the differences among the widths into the three lepton families are very small. The corresponding results[2] are shown in Table 4. We also note that the overlap in the hadron tensor between the T and the $B(B^*)$ wave function slightly favors the pseudoscalar mesons. Anyhow, decays with a single meson in the final state are suppressed by at least

---

[2] The errors quoted correspond to the uncertainties of the Monte Carlo numerical integration.

Table 5

Largest decay widths, in units of 10^{-15} GeV, for the processes described by Fig. 3(b). Here $\ell = e, \mu$.

Final state	$\Gamma [10^{-15}$ GeV$]$	Final state	$\Gamma [10^{-15}$ GeV$]$
$B^{*-} D^{*+} \ell^- \bar{\nu}_\ell$ $\bar{B}^{*0} D^{*0} \ell^- \bar{\nu}_\ell$	9.02 ± 0.07	$B^{*-} D^{*+} \tau^- \bar{\nu}_\tau$ $\bar{B}^{*0} D^{*0} \tau^- \bar{\nu}_\tau$	1.55 ± 0.01
$B^{*-} D^+ \ell^- \bar{\nu}_\ell$ $\bar{B}^{*0} D^0 \ell^- \bar{\nu}_\ell$	3.59 ± 0.03	$B^{*-} D^+ \tau^- \bar{\nu}_\tau$ $\bar{B}^{*0} D^0 \tau^- \bar{\nu}_\tau$	0.727 ± 0.005
$B^- D^{*+} \ell^- \bar{\nu}_\ell$ $\bar{B}^0 D^{*0} \ell^- \bar{\nu}_\ell$	4.63 ± 0.05	$B^- D^{*+} \tau^- \bar{\nu}_\tau$ $\bar{B}^0 D^{*0} \tau^- \bar{\nu}_\tau$	0.86 ± 0.007
$B^- D^+ l^- \bar{\nu}_l$ $\bar{B}^0 D^0 \ell^- \bar{\nu}_\ell$	1.92 ± 0.02	$B^- D^+ \tau^- \bar{\nu}_\tau$ $\bar{B}^0 D^0 \tau^- \bar{\nu}_\tau$	0.409 ± 0.003

Table 6

Largest decay widths, in units of 10^{-15} GeV, for the processes described by Fig. 4.

Final state	$\Gamma [10^{-15}$ GeV$]$	Final state	$\Gamma [10^{-15}$ GeV$]$
$B^{*-} D^{*+} D_s^-$ $\bar{B}^{*0} D^{*0} D_s^-$	4.00 ± 0.06	$B^- D^{*+} D_s^{*-}$ $\bar{B}^0 D^{*0} D_s^{*-}$	3.15 ± 0.05
$B^{*-} D^{*+} D_s^{*-}$ $\bar{B}^{*0} D^{*0} D_s^{*-}$	6.50 ± 0.09	$B^- D^+ D_s^{*-}$ $\bar{B}^0 D^0 D_s^{*-}$	1.20 ± 0.02
$B^{*-} D^+ D_s^-$ $\bar{B}^{*0} D^0 D_s^-$	2.57 ± 0.04	$B^{*-} D^{*+} \rho^-$	3.57 ± 0.09
		$B^{*-} D^{*+} \pi^-$	1.28 ± 0.03
$B^{*-} D^+ D_s^{*-}$ $\bar{B}^{*0} D^0 D_s^{*-}$	2.32 ± 0.03	$B^{*-} D^+ \rho^-$	1.70 ± 0.04
		$B^{*-} D^+ \pi^-$	0.70 ± 0.02
$B^- D^{*+} D_s^-$ $\bar{B}^0 D^{*0} D_s^-$	2.78 ± 0.05	$B^- D^{*+} \rho^-$	2.01 ± 0.05
		$B^- D^{*+} \pi^-$	0.77 ± 0.03

Table 7

Decay widths, in units of 10^{-15} GeV, for the processes described by Fig. 5.

Final state	$\Gamma [10^{-15}$ GeV$]$
$T_{bc} e^- \nu_e$	3.06 ± 0.03
$T_{bc} \mu^- \nu_\mu$	3.02 ± 0.02
$T_{bc} \tau^- \nu_\tau$	1.40 ± 0.01

two orders of magnitude as compared to the semileptonic decays with two final mesons, and the leading non-leptonic modes that are discussed below.

For semileptonic decays involving two mesons in the final state, described by panel (b) of Fig. 3, the processes involving a $b \to c$ vertex are favored compared to those involving a $b \to u$ vertex, due to the larger CKM matrix element $|V_{cb}| \sim 0.041$ compared to $|V_{ub}| \sim 0.0035$ [35]. In Table 5 we show the most favorable channels, the filter being a width larger than $10^9 \, \text{s}^{-1} = 0.66 \times 10^{-15}$ GeV, for the semileptonic decays with two mesons and a light $\ell = e, \mu$ lepton in the final state. Though much smaller, we also give the widths for the corresponding channels with a final τ since they could be interesting in the context of studies of lepton-flavor universality violation. Due to spin recoupling coefficients, the largest decay widths appear for vector mesons in the final state. In short, the largest preferred semileptonic decay are $B^{(*)} D^{(*)} \ell \bar{\nu}_\ell$ with the various combinations of spins for the mesons, and $\ell = e, \mu$.

Table 6 displays now the most important nonleptonic decay modes. All of them contain a $b \to c$ vertex and an a_1 factor, and the dominant ones have a $D_{(s)}^{(*)}$ meson in the final state. Once again vector mesons are favored in the final state. As a consequence of the factorization approximation, processes with D_s or a light meson final states arising from vacuum have decay widths comparable to the corresponding semileptonic decay. This is due to the large value of the Cabibbo allowed CKM matrix elements $|V_{cs}| \sim |V_{ud}| \sim 0.97$ [35] and the fact that the hadronic matrix elements are proportional to a_1^2 in those cases. Decay channels not shown in Tables 5 and 6 are suppressed by at least one order of magnitude. For instance, final states with J/Ψ or η_c mesons, are suppressed by more than one order of magnitude since their widths are proportional to $|V_{cd}|^2 a_2^2$. According to our study, the promising final states among the nonleptonic decays are $\bar{B}^{*-} D^{*+} D_s^{*-}$, $\bar{B}^{*0} D^{*0} D_s^{*-}$, and $\bar{B}^{*-} D^{*+} \rho^-$.

Finally, in Table 7 we show the results for the semileptonic decay corresponding to Fig. 5 with a $J^P = 0^+$ T_{bc} isoscalar tetraquark in the final state. In our calculation, the total semileptonic decay width with a final $J^P = 0^+$ T_{bc} isoscalar tetraquark turns out to be

7.5×10^{-15} GeV, in clear disagreement with the result of Ref. [17] obtained using a QCD three-point sum rule approach.

The total decay width of the T_{bb}^- tetraquark, as calculated in this work, is of the order of $\Gamma \approx 87 \times 10^{-15}$ GeV, which means a lifetime $\tau \approx 7.6$ ps. This lifetime is one order of magnitude larger than the simplest guess-by-analogy estimation of 0.3 ps of Ref. [7].

4. Summary and outlook

We have presented the first comprehensive study of the flavor-exotic $J^P = 1^+$ T_{bb}^- isoscalar tetraquark. It includes an accurate solution of the four-body problem within a quark model, which characterizes the structure of the state, and an estimate of the lifetime and of the rates for the leading semileptonic and non-leptonic decay modes which are the most promising final states where the tetraquark should be looked for. We have shown how pairwise interactions based on color-octet exchange induce mixing between the $\bar{3}3$ and $6\bar{6}$ states in the $QQ - \bar{q}\bar{q}$ basis, enhancing the $\bar{3}3$ components for larger values of M_Q due to the attractive chromoelectric interaction of the QQ pair that it is absent in the $Q\bar{q}$ threshold. This result is only valid in the bottom sector. In the charm sector, the binding mechanism is different: the $\bar{3}3$ and $6\bar{6}$ components have a similar probability and are mixed by the chromomagnetic interaction. We have shown how the structure of the T_{QQ} state evolves from a molecular-like system to a compact-like structure when moving from the charm to the bottom sector.

For the first time, the lifetime of the T_{bb}^- tetraquark has been calculated in a quark model beyond simple guess-by-analogy estimations. The total decay width of the T_{bb}^- found in this work is $\Gamma \approx 87 \times 10^{-15}$ GeV, corresponding to a lifetime $\tau \approx 7.6$ ps. The promising final states are $\bar{B}^{*-} D^{*+} l^- \bar{\nu}_\ell$ and $\bar{B}^{*0} D^{*0} \ell^- \bar{\nu}_\ell$ among the semileptonic decays, and $\bar{B}^{*-} D^{*+} D_s^{*-}$, $\bar{B}^{*0} D^{*0} D_s^{*-}$, and $B^{*-} D^{*+} \rho^-$ among the nonleptonic ones. The $T_{bc}^0 \ell^- \nu_\ell$ semileptonic decay is also relevant but in our calculation is not dominant.

Our study complements recent estimates for the production cross sections of T_{bb} tetraquarks based on Monte Carlo event generators pointing towards an excellent discovery potential in ongoing and forthcoming proton-proton collisions at the LHC [40]. The possible formation of this state in relativistic heavy-ion collisions at the LHC has also been recently discussed in detail within the quark coalescence model using realistic model wave functions with good prospects [41].

The spectroscopy of exotic states with hidden heavy flavor has revealed how interesting the interaction of heavy hadrons is, with presumably a long-range part of Yukawa type, and a short-range part mediated by quark-quark and quark-antiquark forces. A new sector with stable flavor-exotic states, such as the T_{bb}, remains to be investigated. An experimental effort towards the detection of this compact tetraquark states is now timely. Its existence is essential to validate our understanding of low-energy QCD in the multiquark sector.

Note added

A long lifetime for the T_{bb}^- tetraquark can ease its detection through the method of "displaced vertex" proposed in [42]. We thank A. Ali for calling our attention on this article.

Acknowledgements

References

[1] H.-X. Chen, W. Chen, X. Liu, S.-L. Zhu, Phys. Rep. 639 (2016) 1;
R.A. Briceño, et al., Chin. Phys. C 40 (2016) 042001;
J.-M. Richard, Few-Body Syst. 57 (2016) 1185;
R.F. Lebed, R.E. Mitchell, E.S. Swanson, Prog. Part. Nucl. Phys. 93 (2017) 143;
A. Ali, J.S. Lange, S. Stone, Prog. Part. Nucl. Phys. 97 (2017) 123;
A. Esposito, A. Pilloni, A.D. Polosa, Phys. Rep. 668 (2017) 1.
[2] R.L. Jaffe, Phys. Rev. D 15 (1977) 267;
R.L. Jaffe, Phys. Rev. D 15 (1977) 281.
[3] J.D. Weinstein, N. Isgur, Phys. Rev. D 41 (1990) 2236.
[4] J.-P. Ader, J.-M. Richard, P. Taxil, Phys. Rev. D 25 (1982) 2370.
[5] A. Francis, R.J. Hudspith, R. Lewis, K. Maltman, Phys. Rev. Lett. 118 (2017) 142001.
[6] P. Junnarkar, N. Mathur, M. Padmanath, Phys. Rev. D 99 (2019) 034507.
[7] M. Karliner, J.L. Rosner, Phys. Rev. Lett. 119 (2017) 202001.
[8] E.J. Eichten, C. Quigg, Phys. Rev. Lett. 119 (2017) 202002.
[9] P. Bicudo, K. Cichy, A. Peters, M. Wagner, Phys. Rev. D 93 (2016) 034501.
[10] J. Vijande, A. Valcarce, N. Barnea, Phys. Rev. D 79 (2009) 074010.
[11] J.-M. Richard, A. Valcarce, J. Vijande, Phys. Rev. C 97 (2018) 035211.
[12] S.-Q. Luo, K. Chen, X. Liu, Y.-R. Liu, S.-L. Zhu, Eur. Phys. J. C 77 (2017) 709.
[13] M.-L. Du, W. Chen, X.-L. Chen, S.-L. Zhu, Phys. Rev. D 87 (2013) 014003.
[14] A. Czarnecki, B. Leng, M.B. Voloshin, Phys. Lett. B 778 (2018) 233.
[15] R. Aaij, et al., LHCb Collaboration, Phys. Rev. Lett. 119 (2017) 112001.
[16] Y. Xing, R. Zhu, Phys. Rev. D 98 (2018) 053005.
[17] S.S. Agaev, K. Azizi, B. Barsbay, H. Sundu, Phys. Rev. D 99 (2019) 033002.
[18] J. Vijande, A. Valcarce, Phys. Rev. C 80 (2009) 035204.
[19] J. Vijande, A. Valcarce, Symmetry 1 (2009) 155.
[20] E. Hiyama, A. Hosaka, M. Oka, J.M. Richard, Phys. Rev. C 98 (2018) 045208.
[21] M. Oka, S. Maeda, Y.R. Liu, Int. J. Mod. Phys. Conf. Ser. 49 (2019) 196004.
[22] C. Semay, B. Silvestre-Brac, Z. Phys. C 61 (1994) 271.
[23] J.-M. Richard, A. Valcarce, J. Vijande, Phys. Lett. B 774 (2017) 710.
[24] D. Janc, M. Rosina, Few-Body Syst. 35 (2004) 175.
[25] J.L. Ballot, J.-M. Richard, Phys. Lett. B 123 (1983) 449;
S. Zouzou, B. Silvestre-Brac, C. Gignoux, J.-M. Richard, Z. Phys. C 30 (1986) 457;
D.M. Brink, F. Stancu, Phys. Rev. D 49 (1994) 4665.
[26] M. Harvey, Nucl. Phys. 352 (1981) 301.
[27] Y. Ikeda, B. Charron, S. Aoki, T. Doi, T. Hatsuda, T. Inoue, N. Ishii, K. Murano, H. Nemura, K. Sasaki, Phys. Lett. B 729 (2014) 85.
[28] H.J. Lipkin, Phys. Lett. B 172 (1986) 242.
[29] C. Quigg, in: 53rd Rencontres de Moriond QCD High Energy Interactions Conference, La Thuile, Italy, 2018, arXiv:1804.04929 [hep-ph].
[30] E. Hernández, J. Nieves, J.M. Verde-Velasco, Phys. Rev. D 74 (2006) 074008.
[31] E. Hernández, J. Vijande, A. Valcarce, to be published.
[32] D. Ebert, R.N. Faustov, V.O. Galkin, Phys. Rev. D 68 (2003) 094020.
[33] M.A. Ivanov, J.G. Körner, P. Santorelli, Phys. Rev. D 73 (2006) 054024.
[34] P. Colangelo, F. De Fazio, Phys. Rev. D 61 (2000) 034012.
[35] M. Tanabashi, et al., Phys. Rev. D 98 (2018) 030001.
[36] M. Artuso, et al., CLEO Collaboration, Phys. Rev. Lett. 95 (2005) 251801.
[37] D. Becirevic, Ph. Boucaud, J.P. Leroy, V. Lubicz, G. Martinelli, F. Mescia, F. Rapuano, Phys. Rev. D 60 (1999) 074501.
[38] T.F. Caramés, J. Vijande, A. Valcarce, Phys. Rev. D 99 (2019) 014006.
[39] A. Francis, R.J. Hudspith, R. Lewis, K. Maltman, Phys. Rev. D 99 (2019) 054505.
[40] A. Ali, Q. Qin, W. Wang, Phys. Lett. B 785 (2018) 605.
[41] J. Hong, S. Cho, T. Song, S.-H. Lee, Phys. Rev. C 98 (2018) 014913;
S. Cho, et al., ExHIC Collaboration, Phys. Rev. C 84 (2011) 064910;
C.E. Fontoura, G. Krein, J. Vijande, A. Valcarce, Phys. Rev. D 99 (2019) 094037.
[42] T. Gershon, A. Poluektov, JHEP 1901 (2019) 019.